Transonic Flow about Two-Dimensional Airfoils by Relaxation Procedures

J. L. STEGER* AND H. LOMAX†
NASA Ames Research Center, Moffett Field, Calif.

A successive over-relaxation procedure has been developed to treat the inviscid, fully nonlinear, potential equations governing compressible flow. The procedure is designed to compute embedded shock waves and adjust to the Kutta condition during the course of the iterations. Adjustment to the Kutta condition, convergence rate control and other data handling are accomplished in a practical fashion by means of interacting graphics provided by a cathode-ray tube coupled to the computer. The procedure has been applied to blunt-nosed, lifting airfoils in a subsonic freestream. Calculated results are compared to exact theories and experiment.

Introduction

FINITE-DIFFERENCE solutions for transonic-flow simulation can be obtained by differencing the time-dependent partial differential equations or by differencing the steady-state equations using relaxation techniques. The former approach has been studied and reported by Magnus and Yoshihara,[1] Sills,[2] and Grossman and Moretti.[3] Its use does not require the assumption that a steady-state solution exists. However, it does require the assumption (or proof) that if an oscillating flow is the exact solution, the differencing approximation can produce it without introducing spurious damping. The approach using relaxation has been examined by Murman and Cole,[4] Murman and Krupp,[5] Steger,[6] and by Steger and Lomax.[7] Its use requires the assumption that a steady-state solution does exist either at or near the proposed boundary conditions, where "near" is associated in some sense with the truncation errors introduced by the numerical approximation.

This paper continues the study of transonic flow using the concepts of relaxation. As in our previous publication, the basic partial differential equations are the fully nonlinear, inviscid, compressible-flow equations, written in this case for the velocity potential. Unlike our previous publication, we are no longer restricted by the assumption of thin-airfoil theory and consider airfoils having both camber and angle of attack. The two major assumptions are that the embedded shock is weak (therefore the potential equations are valid) and that boundary-layer effects can be neglected. Fortunately, these assumptions are least restrictive when the flow is most nearly shock free.

Coordinate System

The most difficult part of the problem of calculating flowfields about general bodies is the task of inserting the boundary conditions into the finite-differencing grid. This insertion is generally accomplished by data interpolation, local mesh refinements, coordinate transformations or a combination of these. Coordinate transformations that force the boundary of the body to lie along the edge of a grid are extremely attractive. We use this concept with the simplifying approximation that the transformation is only required to place the body close to the edge of a grid.

Consider the blunt plate described by the line ABCDE in Fig. 1. We will refer to this plate as a control surface. The nose of the control surface corresponds closely (in many cases exactly) to the nose of the airfoil, while the aft portion of the airfoil lies within the control surface. The boundary conditions describing the shape of the airfoil section are projected onto the control surface in a manner similar to that used to satisfy the tangency condition in second-order, thin-airfoil theory. The curvature of the control surface does not change sign in proceeding from A to E so that a body coordinate system (sometimes referred to as boundary-layer coordinates, see Hayes and Probstein[8]) and a Cartesian-coordinate system have a one-to-one mapping. The field exterior to the control surface is covered by a rectangular grid in the body coordinate system as shown in Fig. 2. This "unwraps" the airfoil so that its upper and lower surfaces lie along a line close to the bottom edge of the grid.

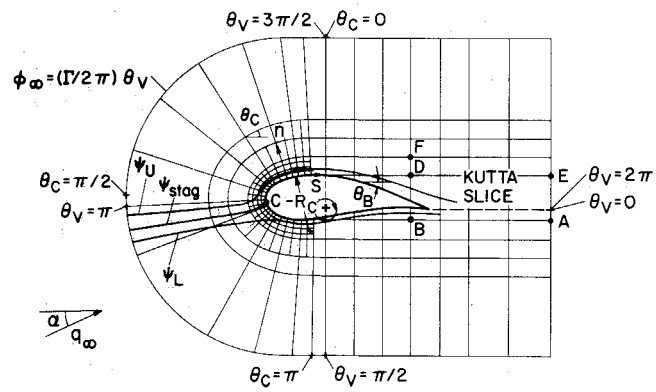

Fig. 1 Control-surface coordinate system.

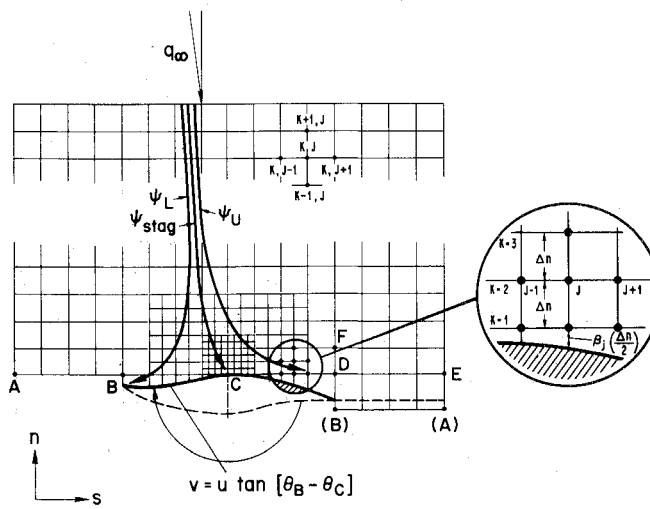

Fig. 2 Control-surface coordinate system unwrapped to form finite difference grid.

Presented as Paper 71-569 at the AIAA 4th Fluid and Plasma Dynamics Conference, Palo Alto, Calif., June 21–23, 1971; submitted July 6, 1971; revision received September 13, 1971.

Index category: Subsonic and Transonic Flow.

* Research Scientist. Associate Member AIAA.

† Chief, Computational Fluid Dynamics Branch. Member AIAA.

Basic Equations

The equations for the disturbance (not total) velocity potential for an inviscid compressible flow can assume the following form when written in terms of body coordinates:

$$\left(\frac{a^2-U^2}{H}\right)\left[\frac{1}{H}\frac{\partial^2\phi}{\partial s^2}+\frac{\partial\phi}{\partial s}\frac{\partial}{\partial s}\left(\frac{1}{H}\right)\right]+(a^2-V^2)\frac{\partial^2\phi}{\partial n^2}-\frac{2UV}{H}\frac{\partial^2\phi}{\partial s\,\partial n}-\frac{1}{HR_c}\left[(a^2-U^2)\frac{\partial\phi}{\partial n}+\frac{2UV}{H}\frac{\partial\phi}{\partial s}\right]=0 \tag{1}$$

$$a^2=a_\infty{}^2-[(\gamma-1)/2](U^2+V^2-q_\infty{}^2) \tag{2}$$

$$U=q_\infty\cos(\theta_c-\alpha)+(1/H)\,\partial\phi/\partial s \tag{3a}$$

$$V=-q_\infty\sin(\theta_c-\alpha)+\partial\phi/\partial n \tag{3b}$$

The s and n coordinates represent, respectively, distances along and normal to the blunt control surface shown in Fig. 1. Notice that $\theta_c(s)$ is the angle that the s coordinate makes with an intersecting x coordinate in a reference Cartesian system, and $R_c(s)$ is the radius of curvature of a point on the control surface. The radius of curvature of an arbitrary point in the field is

$$R(s,n)=R_c(s)-n \tag{4}$$

The angle of attack α is the angle that q_∞ makes with the x coordinate of the reference Cartesian system used to define $\theta_c(s)$. Selected sign conventions for $\theta_c(s)$, $R_c(s)$ and α are shown in Fig. 1. The velocities U and V are total (not disturbance) velocity components that lie along the s and n coordinates, respectively, and $H=R/R_c$.

The boundary condition for flow tangency can be satisfied by requiring that along the body

$$V=U\tan[\theta_B(s)-\theta_c(s)] \tag{5}$$

where $\theta_B(s)$ is defined as $\theta_c(s)$ except that it is referenced to the actual body rather than to the control surface. Clearly, wherever the control surface coincides with the body, $\theta_B(s)=\theta_c(s)$, and V is zero since it represents the velocity component normal to the body. Far from the body the velocity components are given by

$$U=q_\infty\cos(\theta_c-\alpha);\qquad V=-q_\infty\sin(\theta_c-\alpha)$$

and

$$\partial\phi/\partial n=\partial\phi/\partial s=0 \tag{6}$$

For nonlifting airfoils Eq. (6) is satisfied by requiring that $\phi_\infty=0$. This can be generalized to lifting cases by the condition that

$$\phi_\infty=(\Gamma/2\pi)\tan^{-1}[y_\infty(1-M_\infty^2)^{1/2}/x_\infty]=(\Gamma/2\pi)\,\theta_v \tag{7}$$

where Γ is a constant representing the circulation caused by the lift, and the sign convention for θ_v is illustrated in Fig. 1. The value of Γ is made unique by forcing the solution to satisfy the Kutta condition at the trailing edge of the airfoil.

Difference Equations

The grid for the finite-differencing scheme is shown in Fig. 2. The (s,n) origin is placed at the point A and uniform mesh steps Δs and Δn are used such that

$$\begin{aligned} s&=(J-1)\cdot\Delta s \qquad 1\le J\le JMAX\\ n&=(K-1)\cdot\Delta n \qquad 1\le K\le KMAX\end{aligned} \tag{8}$$

Then

$$\phi_{KJ}\equiv\phi(s,n)$$

The (K,J) indices are so ordered to follow matrix convention. Note that they are the reverse of the (s,n) ordering in the analytic description of ϕ.

Second-order differencing schemes are used throughout and depend on whether the flow at a given point is subsonic or supersonic. For subsonic flow, the difference approximations are central schemes given by

$$\left.\frac{\partial^2\phi}{\partial s^2}\right|_{,J}=\frac{(\phi_{K,J+1}-2\phi_{K,J}+\phi_{K,J-1})}{(\Delta s)^2} \tag{9a}$$

$$\left.\frac{\partial\phi}{\partial s}\right|_{K,J}=\frac{(\phi_{K,J+1}-\phi_{K,J-1})}{2\Delta s} \tag{9b}$$

$$\left.\frac{\partial^2\phi}{\partial s\,\partial n}\right|_{K,J}=\frac{(\phi_{K+1,J+1}+\phi_{K-1,J-1}-\phi_{K+1,J-1}-\phi_{K-1,J+1})}{4\Delta s\,\Delta n} \tag{9c}$$

$$\left.\frac{\partial^2\phi}{\partial n^2}\right|_{K,J}=\frac{(\phi_{K+1,J}-2\phi_{K,J}+\phi_{K-1,J})}{(\Delta n)^2} \tag{10a}$$

$$\left.\frac{\partial\phi}{\partial n}\right|_{K,J}=\frac{(\phi_{K+1,J}-\phi_{K-1,J})}{2\Delta n} \tag{10b}$$

In the regions having supersonic flow, Eqs. (10) are still used for the n derivatives, but one-sided schemes (as first successfully used by Murman and Cole[4]) replace the s differencing to prevent upstream-wave propagation. The derivatives are backward differenced for the supersonic region above the airfoil and forward differenced for the supersonic region below the airfoil (see Fig. 2). The backward differencing schemes used are

$$\left.\frac{\partial^2\phi}{\partial s^2}\right|_{K,J}=\frac{2\phi_{K,J}-5\phi_{\ ,J-1}+4\phi_{K,J-2}-\phi_{K,J-3}}{(\Delta s)^2} \tag{11a}$$

$$\left.\frac{\partial\phi}{\partial s}\right|_{K,J}=\frac{5\phi_{K,J-1}-8\phi_{K,J-2}+3\phi_{K,J-3}}{2\Delta s} \tag{11b}$$

$$\left.\frac{\partial^2\phi}{\partial s\,\partial n}\right|_{K,J}=\frac{1}{4\Delta n\,\Delta s}[3(\phi_{K+1,J}-\phi_{K-1,J})-4(\phi_{K+1,J-1}-\phi_{K-1,J-1})+(\phi_{K+1,J-2}-\phi_{K-1,J-2})] \tag{11c}$$

The forward differencing schemes are equivalent to Eqs. (11) but are derived for the opposite direction.

Two remarks should be made at this point. First, the change from central to skewed differencing is not programed to take place precisely at the sonic line. Rather a stable iterative procedure is maintained by a test on the term (a^2-U^2) and the transfer to skew differencing is made when this term becomes negative. This criterion does not fully prevent upstream wave propagation in the vicinity of the sonic line, but for transonic airfoil problems, the velocity component along an s coordinate is nearly the total velocity itself in regions where the flow is supersonic. A transfer back to central differencing occurs downstream of the shock when (a^2-U^2) again becomes positive. Second, the transfer of differencing schemes is made as the relaxation calculations proceed from a subsonic to a supersonic region but for the $\partial\phi/\partial s$ and $\partial^2\phi/\partial s\,\partial n$ terms it is not made abruptly. A factor b is formed where

$$b=1+80(a^2-U^2)/q_\infty^2 \tag{12a}$$

and is bounded by computer logic such that

$$0\le b\le 1 \tag{12b}$$

The derivatives are than evaluated using the expressions

$$\left.\begin{aligned}\frac{\partial\phi}{\partial s}&=b\left.\frac{\partial\phi}{\partial s}\right|_{\text{central}}+(1-b)\left.\frac{\partial\phi}{\partial s}\right|_{\text{skew}}\\ \frac{\partial^2\phi}{\partial s\,\partial n}&=b\left.\frac{\partial^2\phi}{\partial s\,\partial n}\right|_{\text{central}}+(1-b)\left.\frac{\partial^2\phi}{\partial s\,\partial n}\right|_{\text{skew}}\end{aligned}\right\} \tag{13}$$

The differencing for $\partial^2\phi/\partial s^2$ was abruptly changed from Eq. (9a) to Eq. (11a) but because this term is always multiplied by the test factor (a^2-U^2), transition occurs smoothly in the actual calculations.

In formulating the test for (a^2-U^2), central differencing is always used to evaluate the U component. If, using this information, the term (a^2-U^2) is negative, the velocities are re-evaluated using the skewed scheme. The supersonic differencing is then retained regardless of its effect on the sign of (a^2-U^2); however, if the re-evaluated (a^2-U^2) term is now positive, it is set equal to zero. Procedures such as this, and the choice of certain parameters in the computation [such as 80 in Eq. (12)] are certainly subjective, but their effectiveness has been judged to be satisfactory

by monitoring the relaxation process through interactive graphics.

The tangency-boundary condition given by Eq. (5) can be written

$$\frac{\partial\phi}{\partial n}-q_\infty\sin(\theta_c-\alpha)=\left[\frac{1}{H}\frac{\partial\phi}{\partial s}+q_\infty\cos(\theta_c-\alpha)\right]\tan(\theta_B-\theta_c)$$

where $H=1$ on the body. The derivatives are differenced using

$$\left.\frac{\partial\phi}{\partial n}\right|_{1,J}=\frac{-(3+\beta_J)\phi_{1,J}+(4+2\beta_J)\phi_{2,J}-(1+\beta_J)\phi_{3,J}}{2\Delta n} \quad (14a)$$

and

$$\left.\frac{1}{H}\frac{\partial\phi}{\partial s}\right|_{1,J}=\frac{1}{4\Delta s}\left[(2+\beta_J)(\phi_{1,J+1}-\phi_{1,J-1})-\right. \quad (14b)$$

$$\left.\frac{\beta_J}{H_{2,J}}(\phi_{2,J+1}-\phi_{2,J-1})\right] \quad (14b)$$

along the lower mesh line BD in Fig. 2. If this line does not coincide with the body, $\beta_J\Delta n/2$ is the distance between the control surface and the body (see insert in Fig. 2). Equations (14) are used regardless of whether or not the local flow is supersonic.

In our calculations the boundary conditions at infinity are replaced by imposing conditions on ϕ about 3 chord lengths away from the airfoil. These conditions are given by using Eq. (7) in which x_∞ and y_∞ are replaced by the finite lengths chosen. The reliability of this procedure can be determined by comparing solutions computed for different exterior boundary locations. We used, for example, 2.5 and 3.5 chord lengths for the outer boundaries and found no difference between the body pressure distributions that was significant in the scale chosen for the plots presenting our results. This statement is limited, of course, to the Mach number, thickness ratio, and angle-of-attack range covered.

In the nose region of a blunt airfoil, the flow gradients are larger than elsewhere in the field. To increase accuracy, the mesh in the region of the nose is locally refined by halving the grid size twice. As a result there are three grid systems—a major outer system and two embedded finer-mesh systems as shown in Fig. 2. When the grid size is doubled at a given point, the numerical truncation error for the second-order, finite-difference scheme jumps by a factor of 4. This increase is sometimes noticeable in the computed pressure distribution if the grid is changed in a steep flow gradient.

Numerical Calculation of the Kutta Condition

Far from the lifting airfoil, the flow resembles simple vortex flow. The disturbance velocities induced by a vortex go to zero at distances far from the vortex core, but the disturbance velocity potential takes the form given by Eq. (7). Across a slice in the flowfield, the angle θ_v jumps from 0 to 2π, and across this slice ϕ is discontinuous, the magnitude of its jump being equal to Γ. To apply the condition that the pressure is continuous across the Kutta slice, the velocities across the slice must be continuous and therefore are computed from the potential using derivatives that in principle do not cross the cut. In our method, the Kutta slice lies in region $ABDE$ of Fig. 2. Consider the problem of differencing ϕ with respect to n at the point D in the figure. For simplicity, assume points F, D, and B are equally spaced in n. Then, using central differencing we can write

$$(\partial\phi/\partial n)_D=(\phi_F-\phi_B)/2\Delta n$$

where ϕ_B is stored in the row ϕ_1,J at a position representing the point just below D in the unwrapped mesh (see Fig. 1). However, the value stored in ϕ_F is larger by the magnitude Γ than the value "expected" by a Taylor series expansion of data extended from B to F through D. To compensate for the jump in circulation, the derivative is evaluated as follows:

$$(\partial\phi/\partial n)_D=[\phi_F-(\phi_B+\Gamma)]/2\Delta n \quad (15)$$

A procedure equivalent to this, but accounting for the unequal spacing, is followed in computing $\partial\phi/\partial n$ along the lines AB and DE. The details of finding Γ are described in the next section.

Iteration Procedure and Graphic Interaction

The difference equations described previously form a system of nonlinear-algebraic equations that must be solved simultaneously. For this purpose, standard relaxation procedures[9,10] were employed. Both successive point over-relaxation and successive line over-relaxation were tried. The latter was used along vertical lines in the manner described by Murman and Cole[4] and was found to be more efficient with regard to computing time. It is the method used for the calculations reported below.

The efficiency of any over-relaxation process depends on the choice of certain relaxation parameters. This choice, in turn, depends on the eigenvalue structure of the associated matrix[11] generated by the difference equations. Our calculations indicate that acceptable choices of the relaxation parameter are close to 1 for supersonic regions and less than 2 for subsonic regions. These numbers relate to difference equations that have been normalized about the diagonal in the usual way. Strict theoretical justification for these values cannot yet be given, but we include the following remarks. The difference equations formed by using Eqs. (9) and (10) in the subsonic regions are similar to those formed by using the "five-point star" for Laplace's equation, and several simple numerical computations indicate that the eigenvalue spectrums are similar. The Laplace equation has been thoroughly analyzed and the optimum-SLOR-relaxation parameter for it is known to be slightly less than 2 for calculations using a large number of points. On the other hand, the difference equations formed by using Eqs. (10) and (11) in the supersonic regions generate an associated matrix which is a sum of tridiagonal and lower triangular matrices, and the optimum choice of a relaxation parameter for a normalized lower triangular set of equations is 1. Of course, these concepts only lead to primitive guidelines, and truly optimum-relaxation parameters cannot be defined until the eigenvalue spectrums of the difference equations are tabulated for a variety of flow conditions.

Superimposed on the over-all relaxation procedure is the iterative solution for the proper airfoil circulation, that is, the correct choice of the constant Γ. The actual computational technique used is to couple the computer with an interactive-cathode ray tube and to display, as the computations proceed, the value of the relaxation parameters, the circulation, and the maximum residuals as well as the entire pressure distribution on the airfoil. Values of the circulation and the relaxation parameters are changed interactively as the relaxation is proceeding. The final solution is assumed to be close to that which exists when the maximum residual is "sufficiently" small; this is referred to as the converged solution. The final choice of Γ is, of course, that value which makes the pressure continuous at the trailing edge in the converged solution.

In practice, this interactive procedure has proven to be satisfactory provided Γ is not allowed to change too rapidly. In other words, it can be a bad strategy (one which can lead to numerical instability) if the pressure at the trailing edge is continuously forced to be zero in the intermediate stages of relaxation. The interactive capability greatly simplifies the implementation of superior strategies for relaxing to the proper circulation as the nonlinear flowfield is guided toward convergence. Interactive graphic capability rather obviously also permits one to proceed quickly from one converged solution to another, representing a different Mach number, angle of attack, or airfoil shape.

Execution times vary depending on the amount of circulation and on the initial estimate for Γ. Some rather straightforward attempts have been made to speed up the calculations within the framework of the technique described. For example, moderate decreases in running time were obtained by iterating the finer nose mesh more frequently than the outer mesh. Work along these lines is continuing and improvements in efficiency are expected. At present a typical case—for example, an NACA 0012 airfoil at $M_\infty=0.75$ and $\alpha=2°$—converges in 20 min on an IBM 360–67 computer. This is the worst case in the sense that for this particular calculation the circulation was initially taken to be zero.

Discussion of Results

The computer program for the relaxation process contains a geometry package that requires the specification of arc length, slope and radius of curvature of the airfoil. Because many airfoils are defined by only a table of nonuniformly spaced ordinates, the evaluation of these geometric quantities is often the largest source of error. Fortunately, the NACA 4- and 5-digit airfoil series have analytic specifications, and also have been investigated experimentally in the transonic range. Further, two "exact" subcritical solutions, for both a lifting and a nonlifting case, are given by Lock[12] using the method of Sells.[13]

In order to evaluate our computing capability for arbitrary shapes, the analytic NACA 0012 was represented by a table of data for x, y, θ, and R, equally spaced in the variable $1-\cos[x(\pi/2)]$, $0 \leq x \leq 1$. Arc length was numerically evaluated and then interpolated for an equispaced grid in the control surface body coordinate system. Simple quadratic interpolation was used to re-valuate θ and R at the grid locations. Using this type of airfoil representation, the relaxation procedure described above was used to compute the pressure distribution for $\alpha = 2°$, $M_\infty = 0.63$. The results are shown in Fig. 3 and are generally in good agreement with those given by Lock. The slight discrepancy at the trailing edge can be attributed to a lack of refinement of the mesh near the rear stagnation point.

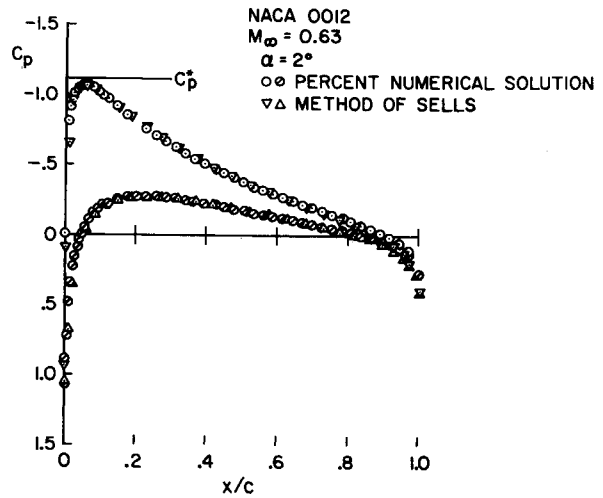

Fig. 3 Subcritical comparison, flow with circulation.

Figure 4 shows a comparison between our numerical solution and the experimental data presented by DePaul and Dyment[14] for the NACA 0012 airfoil at $\alpha = 0°$ and $M_\infty = 0.864$. The wind-tunnel data are for low Reynolds number (1.1×10^6) and the boundary layer was tripped. The numerical calculations

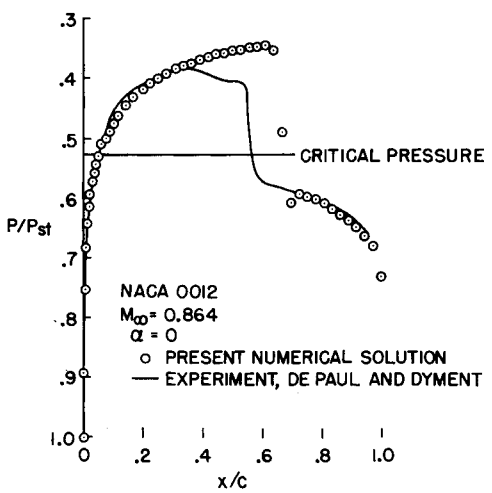

Fig. 4 Comparison between experimental data and numerical results for supercritical flow.

predict the shock to be downstream of the experimental location by about 10% of the chord length. As shock waves increase in strength, this type of discrepancy is typical of comparisons between inviscid solutions and low Reynolds number wind-tunnel data.

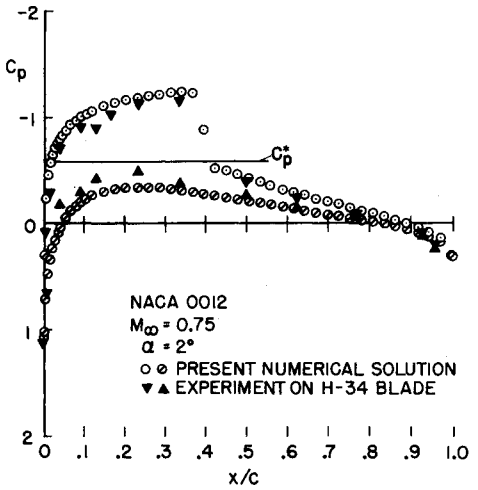

Fig. 5 Supercritical flow for NACA 0012.

Lock [12] has suggested that the NACA 0012 airfoil be used as a test case for transonic flow investigations because of its analytic description. Anticipating more and better experimental data for this profile, we have included two additional supercritical calculations shown in Figs. 5 and 6. Data[15] from a

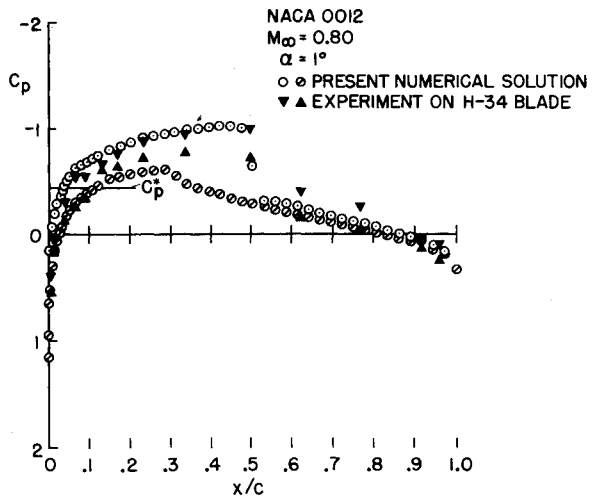

Fig. 6 Supercritical solution for NACA 0012.

production H—34 helicopter blade, which is essentially an NACA 0012 profile with a trailing-edge tab, is also shown for comparison. Two numerical solutions for the thicker NACA 0015 airfoil at supercritical speeds are also shown in Figs. 7 and 8. Data taken by Graham et al.[16] in 1945 is in qualitative agreement.

The hodograph solutions of the quasi-elliptic profiles of Nieuwland[17] and the NLR furnish more "exact" data; and the profile geometries, including slope and curvature, are extensively tabulated, although the tabulations have nonuniform spacing. A supercritical case for an airfoil from the quasi-elliptic series is shown in Fig. 9, and is compared with a hodograph solution tabulated by Lock.[12] Notice that the numerical simulation appears to predict two weak shocks. This is typical of our comparisons with the shock-free quasi-elliptic profiles, although one weak shock is usually observed, not two.

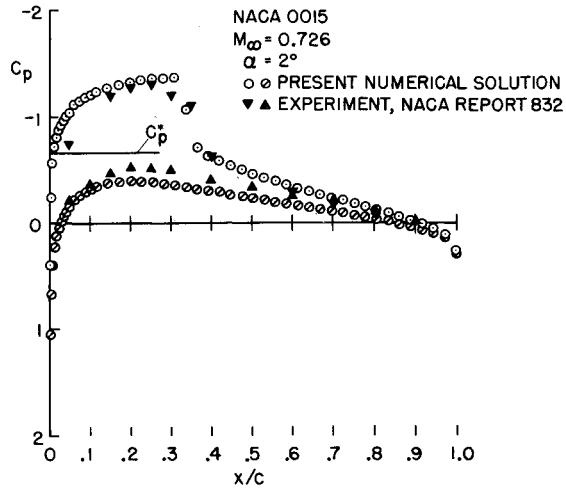

Fig. 7 Supercritical solution for NACA 0015.

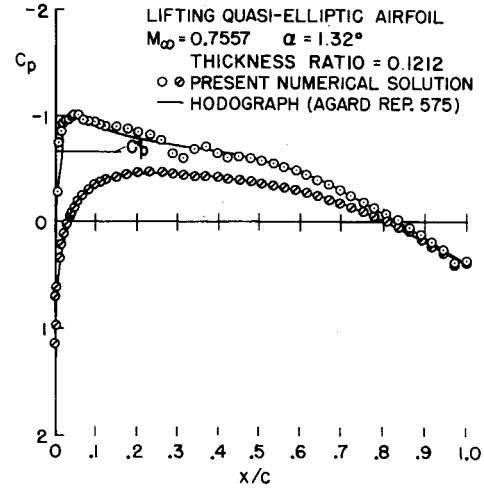

Fig. 9 Comparison of numerical solution with exact hodograph, shock-free solution.

As a final comparison, we have included results for an NACA 64A410 airfoil. This airfoil has inadequate geometric specifications for flow calculations of the type being described. Only a sparse list of ordinates is available to define the profile and it is impossible to numerically compute an accurate and unique table of surface curvatures using these data. Of course, smoothing or least-squares-type numerical procedures can be applied, but then the curvature in the nose region becomes a function of the numerical technique. Figure 10 compares our numerical solution for the supercritical flow about this airfoil with the numerical solution presented by Magnus and Yoshihara.[1] The experimental data of Stivers[18] are also shown in the figure. Both numerical solutions show the typical discrepancy with wind-tunnel data for shock location, and this can be attributed to boundary-layer interaction. The numerical calculations appear to generate too much lift on the lower surface, and this may be caused, we think, by the poor description of the nose region of the airfoil.

Conclusions

Accurate numerical simulations of two-dimensional, inviscid, transonic, supercritical flows can be obtained for cambered, blunt-nosed airfoils at angle of attack. The solutions can be computed using standard methods of relaxation provided the differencing schemes in the supersonic regions do not use values downstream of the vertical line being relaxed. The particular method of relaxation used to obtain the results presented here is not optimum from the viewpoint of efficiency in computer running time, although the use of interactive graphics makes it a practical tool for calculating supercritical flows. The method can also be used for designing airfoils that are optimum under given constraints in inviscid flows, and it is anticipated that families of such airfoils will be developed in the near future.

References

[1] Magnus R. and Yoshihara, H., "Inviscid Transonic Flow over Airfoils," *AIAA Journal*, Vol. 8, No. 12, Dec. 1970, pp. 2157–2162.

[2] Sills, J. A., "Computation of Inviscid, Two-Dimensional Transonic Flows Using a Time-Dependent Finite Difference Method," ERR-FW-806, 1968, General Dynamics, Fort Worth, Texas.

[3] Grossman, B. and Moretti, G., "Time-Dependent Computation of Transonic Flows," AIAA Paper 70–1322, Houston, Texas, 1970.

[4] Murman, E. M. and Cole, J. D., "Calculations of Plane Steady Transonic Flows," *AIAA Journal*, Vol. 9, No. 1, Jan. 1971, pp. 114–121.

[5] Murman, E. M. and Krupp, J. A., "Solution of the Transonic Potential Equations Using a Mixed Finite Difference System, *Proceedings of the Second International Conference on Numerical Methods in Fluid Dynamics*, Vol. 8, Springer-Verlag, New York, 1971, pp. 199–206.

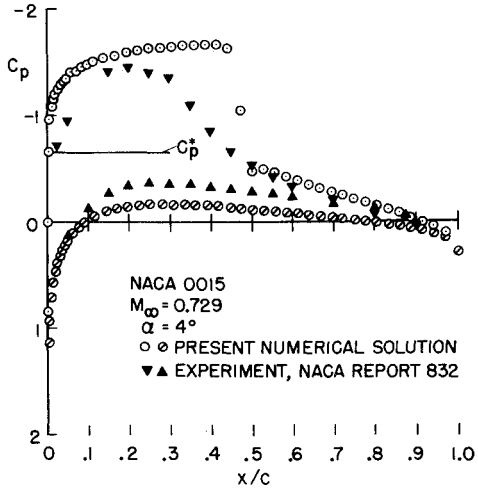

Fig. 8 Supercritical solution for NACA 0015.

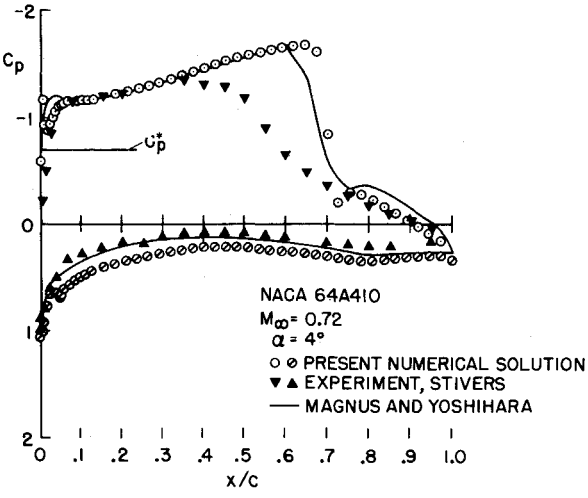

Fig. 10 Comparison of our numerical solution with numerical solution found by Magnus and Yoshihara and with experimental data.

[6] Steger, J. L., "Application of Cyclic Relaxation Procedures to Transonic Flow Fields," Ph.D. thesis, 1969, Iowa State Univ., Ames, Iowa.

[7] Steger, J. L. and Lomax, H., "Generalized Relaxation Methods Applied to Problems in Transonic Flow," *Proceedings of the Second International Conference on Numerical Methods in Fluid Dynamics*, Vol. 8, Springer-Verlag, New York, 1971, pp. 193–198.

[8] Hayes, W. D. and Probstein, R. F., *Hypersonic Flow Theory*, 2nd ed., Vol. 1, Academic Press, New York, 1966.

[9] Wachspress, E. L., *Iterative Solution of Elliptic Systems*, Prentice-Hall, Englewood Cliffs, N.J., 1966.

[10] Varga, R. S., *Matrix Iterative Analysis*, Prentice-Hall, Englewood Cliffs, N.J., 1962.

[11] Lomax, H., "On the Construction of Highly Stable, Explicit, Numerical Methods for Integrating Coupled Ordinary Differential Equations With Parasitic Eigenvalues," TN D-4547, April 1968, NASA.

[12] Lock, R. C., "Test Cases for Numerical Methods in Two-Dimensional Transonic Flows," Rept. 575, 1970, AGARD.

[13] Sells, C. C. L., "Plane Subcritical Flow Past a Lifting Aerofoil," TR. 67146, June 1967, Royal Aircraft Establishment, Farnborough, Hants, England.

[14] DePaul, V. and Dyment, A., "Recherches sur les profils d'aiks en écoulement subsonique élève," *L'Aeronautique et l'Astronautique*, No. 19, 1970, pp. 15–30.

[15] United Aircraft Corp., Sikorsky Aircraft Division, "Two-Dimensional Wind Tunnel Tests of an H-34 Main Rotor Airfoil Section," TRECTR 60-53, 1960.

[16] Graham, D. J., Nitzberg, G. E., and Olson, R. N., "A Systematic Investigation of Pressure Distributions at High Speeds Over Five Representative NACA Low-Drag and Conventional Airfoil Sections," Rept. 832, 1945, NACA.

[17] Nieuwland, G. Y., "Transonic Potential Flow Round a Family of Quasi-Elliptic Aerofoil Sections," NLR-TR T.172, 1967.

[18] Stivers, L. S., Jr., "Effects of Subsonic Mach Numbers of the Forces and Pressure Distributions on Four NACA 64A-Series Airfoil Section at Angles of Attack as High as 28°," TN 3163, March 1954, NACA.